The Structural Basis of Sirtuin Substrate Affinity[†,‡]

Michael S. Cosgrove,[▽,§] Katherine Bever,[▽,∥] Jose L. Avalos,[▽,⊥] Shabazz Muhammad,[▽,∥] Xiangbin Zhang,[▽,∥] and Cynthia Wolberger*[,▽,∥]

Department of Biophysics and Biophysical Chemistry and Howard Hughes Medical Institute, Johns Hopkins School of Medicine, 725 North Wolfe Street, Baltimore, Maryland 21205

Received December 23, 2005; Revised Manuscript Received April 10, 2006

ABSTRACT: Sirtuins comprise a family of enzymes that catalyze the deacetylation of acetyllysine side chains in a reaction that consumes NAD^+. Although several crystal structures of sirtuins bound to non-native acetyl peptides have been determined, relatively little about how sirtuins discriminate among different substrates is understood. We have carried out a systematic structural and thermodynamic analysis of several peptides bound to a single sirtuin, the Sir2 homologue from *Thermatoga maritima* (Sir2Tm). We report structures of five different forms of Sir2Tm: two forms bound to the p53 C-terminal tail in the acetylated and unacetylated states, two forms bound to putative acetyl peptide substrates derived from the structured domains of histones H3 and H4, and one form bound to polypropylene glycol (PPG), which resembles the apoenzyme. The structures reveal previously unobserved complementary side chain interactions between Sir2Tm and the first residue N-terminal to the acetyllysine (position −1) and the second residue C-terminal to the acetyllysine (position +2). Isothermal titration calorimetry was used to compare binding constants between wild-type and mutant forms of Sir2Tm and between additional acetyl peptide substrates with substitutions at positions −1 and +2. The results are consistent with a model in which peptide positions −1 and +2 play a significant role in sirtuin substrate binding. This model provides a framework for identifying sirtuin substrates.

The Sir2[1] family of enzymes, known as sirtuins, catalyze the removal of an acetyl group from the ϵ-amino group of lysine in a reaction that consumes NAD^+ (*1*), releasing nicotinamide, *O*-acetyl-ADP-ribose, and the deacetylated peptide (*2*−*6*). This deacetylation activity is important for a number of biological processes, including transcriptional silencing (*7*), DNA recombination (*8*, *9*), DNA repair (*10*), apoptosis (*11*−*13*), axonal protection (*14*), fat mobilization (*15*), and aging (*16*, *17*). Sirtuins, which are conserved from bacteria to humans, have a variety of physiological substrates that include histones (*1*), acetyl-coA synthetase (*18*), α-tubulin (*19*), myoD (*20*), p53 (*12*, *13*), Foxo3 (*11*, *21*), Ku70 (*22*), and NF-κB (*23*). Many organisms have multiple sirtuin paralogs, some of which differ in subcellular localization (*24*) and, presumably, in substrate specificity. However, the molecular details of how different sirtuins discriminate among substrates have remained elusive.

Crystal structures of several different sirtuins in a variety of liganded states have provided insights into the enzymatic mechanism of NAD-dependent deacetylation (*2*, *25*−*33*). However, the molecular basis of sirtuin substrate selectivity has been more difficult to resolve. Three structures of sirtuins bound to non-native substrates have been reported: that of an archaeal sirtuin to an acetyl peptide derived from the C-terminal regulatory domain of p53 (*27*) and of the yeast HST2 (*31*) and bacterial CobB (*32*) enzymes bound to a peptide derived from the histone H4 tail. These structures show that peptide binding is dominated by the insertion of the acetyllysine into a highly conserved hydrophobic tunnel and by the formation of an enzyme substrate β-sheet, called a β-staple, with peptide residues adjacent to the acetyllysine. The β-sheet interactions between the enzyme and substrate in all three cases involve primarily main chain atoms of the substrate and enzyme, leading to the suggestion that sirtuins possess relatively little substrate specificity or that the determinates of specificity lie outside the conserved catalytic core of the enzyme. While some observations support this view (*32*, *34*, *35*), others do not (*27*, *36*, *37*). For example, recent quantitative steady-state kinetic analyses with three different sirtuin enzymes and several peptide substrates show varying catalytic efficiencies, suggesting that sirtuins do indeed discriminate among substrates (*36*). This is supported by the recent demonstration that the human ortholog, SirT1, can discriminate among peptide substrates in an acetyl peptide library by as much as 20-fold (*37*). In addition, a triple mutation of surface side chain residues in the archaeal

[†] This work was supported in part by a grant from the National Institutes of Health (GM62385) to Jef Boeke and C.W. and by a Ruth L. Kirschstein National Research Service Award to M.S.C.

[‡] Coordinates of Sir2Tm complexes have been deposited in the Protein Data Bank under ID codes 2H2I, 2H2D, 2H2F, 2H2H and 2H2G.

* To whom correspondence should be addressed: 725 N. Wolfe St., Baltimore, MD 21205. Phone: (410) 955-0728. Fax: (410) 614-8648. E-mail: cwolberg@jhmi.edu.

[▽] Department of Biophysics and Biophysical Chemistry.

[§] Current address: Department of Biology, Syracuse University, Syracuse, NY 13244.

[∥] Howard Hughes Medical Institute.

[⊥] Current address: The Rockefeller University, New York, NY 10021.

[1] Abbreviations: Sir2, silent information regulator; NAD^+, nicotinamide adenine dinucleotide; Sir2Tm, Sir2 homologue from *T. maritima*; PPG, polypropylene glycol.

10.1021/bi0526332 CCC: $33.50
Published on Web 05/28/2006

Table 1: Data Collection and Refinement Statistics

	Sir2Tm−PPG	p53-K382ac	p53-K382	H4-K79ac	H3-K115ac
space group	*P*432	$P2_12_12_1$	$P2_12_12_1$	$P2_12_12_1$	$P2_12_12_1$
cell parameters					
a (Å)	133.1	45.2	45.8	46.0	46.2
b (Å)	133.1	58.7	59.0	59.3	58.1
c (Å)	133.1	104.5	105.9	106.2	109.1
resolution (Å)	50−1.94	50−1.83	50−2.3	50−2.0	50−1.63
no. of measured reflections	700216	245614	107741	90761	222888
no. of unique reflections	37913	31371	17279	20296	37292
completeness (%)[a]	99.9 (100)	100 (100)	99.2 (99.2)	98.4 (95.1)	99.9 (100)
average I/σ[a]	41 (10)	24 (5)	29 (7)	21 (4)	26 (4)
multiplicity	18	7.8	6.2	4.5	6.0
mosaicity	0.29	0.36	1.62	0.41	0.80
R_{merge} (%)	7.8 (37)	7.0 (30)	9.2 (39)	6.3 (27)	6.9 (51)
refinement statistics					
$R_{working}$ (%)	18.6	21.7	20.9	21.5	20.6
R_{free} (%)	21.3	22.8	24.9	24.4	22.9
no. of atoms/*B* factors (Å^2)					
protein	1938/26.6	1871/33.7	1835/36.1	1847/26.6	1864/18.3
peptide		115/38.5	66/60.6	68/41.2	54/25.7
water	208 /38.6	95/30.9	100/47.0	165/38.44	252/33.3
Zn ions	1/24.8	1/28.2	1/44.2	1/32.6	2/21.5
rms deviations					
bond lengths (Å)	0.02	0.01	0.01	0.01	0.0005
bond angles (deg)	1.75	1.34	1.08	1.14	1.14

[a] Values in parentheses are for the highest-resolution shell.

Sir2 from *Archaeoglobus fulgidus* increases the affinity of this enzyme for a p53-derived peptide (*27*). However, the rules that govern the substrate specificity of sirtuins have remained unclear, due in part to the lack of a systematic structural analysis of different peptides within a single model system.

In this investigation, we carried out a structural study of peptide recognition by sirtuins using a systematic structural and thermodynamic analysis of peptide binding to the bacterial sirtuin, Sir2Tm, from *Thermatoga maritima*. We report here five structures of Sir2Tm: three bound to different acetylated peptides, one bound to an unacetylated peptide, and one bound to polypropylene glycol, which resembles the apoenzyme. Our analysis of the structures, together with enzymatic and thermodynamic data, reveals structural features suggesting that sirtuins recognize specific substrates by selecting particular amino acid side chains in positions −1 and +2 of the peptide substrate relative to the acetyllysine side chain. These results provide a framework for identifying sirtuin substrates.

MATERIALS AND METHODS

Protein Expression and Purification. The Sir2Tm enzyme from *T. maritima* was expressed in *Escherichia coli* and purified as previously described (*38*). Purified Sir2Tm was dialyzed into 10 mM HEPES (pH 7.4) and concentrated to 16 mg/mL. Site-directed mutagenesis (QuickChange) was used to introduce the N165A and N165D mutations into Sir2Tm. The mutant enzymes were expressed and purified as described for the wild-type enzyme.

The unblocked 18- and 12-residue p53 peptides were synthesized and purified as previously described (*27*). The remaining peptides were synthesized and purified (>95%) by Global Peptide Services, LLC, and were designed on the basis of previous sirtuin−peptide structures to include only portions of the peptide that were ordered in those complexes (*27*, *31*, *32*). To eliminate interference with binding due to the effect of N- and C-terminal charges in the shortened peptides, the N- and C-termini were blocked by acetylation and amidation, respectively.

Crystallization and Data Collection. Stock peptide solutions at concentrations of 40−50 mM were made up in deionized water and brought to neutral pH by the addition of NaOH. Four to five microliters of peptide stock solutions was added to concentrated solutions of Sir2Tm, and the volume was adjusted to give a final Sir2Tm concentration of 10 mg/mL and final peptide concentrations of 4−5 mM. Crystals were grown using the hanging drop method. p53-K382ac and p53-K382 cocrystals were grown in 100 mM CHES (pH 9.6) and 19% PEG 3350. Crystals of histone peptide H3-K115ac in complex with Sir2Tm were grown in 100 mM HEPES (pH 7.5) with 10% PEG 8000. Crystals of histone peptide H4-K79ac in complex with Sir2Tm were grown in 100 mM CHES (pH 9.5) with 1 M K/Na tartarate and 200 mM $LiSO_4$. All peptide cocrystals were flash-frozen in mother liquor containing 20% ethylene glycol.

Sir2Tm−PPG crystals were grown using the hanging drop method with 20 mg/mL Sir2Tm, 2 mM NAD^+, 0.1 M sodium citrate, 1 M Li_2SO_4, 0.5 M $(NH_4)_2SO_4$, 150 mM NaCl, and 4% polypropylene glycol (PPG400). The crystals grew in 7 days and were flash-frozen in Nujol oil.

Structure Determination and Refinement. Diffraction data for the p53-K382ac, H3-K115ac, and H4-K79ac Sir2Tm−peptide complexes were collected at Biocars beamlines 14BMC and 14BMD at the Advanced Photon Source (APS). Diffraction data for the p53−K382 complex and the Sir2Tm−PPG crystals were collected at the National Synchrotron Light Source (NSLS) on beamlines X25 and X4A, respectively. All data were collected with Quantum CCD detectors and reduced with HKL2000 (*39*) and CCP4. Data collection statistics are given in Table 1. The Sir2Tm−PPG structure was determined by molecular replacement with MOLREP (*40*) using the coordinates of the previously determined Sir2-Af1 bound to NAD^+ as a search model (*29*). The structure

was refined with simulated annealing, energy minimization, and individual *B*-factor refinement with a maximum likelihood target using CNS (*41*). The final refined structure contained all 246 amino acids, one Zinc atom, one sulfate ion, 29 atoms of PPG, and 225 waters.

Sir2Tm−peptide complex structures were determined by molecular replacement using as a search model the Sir2Tm−PPG structure separated into large and small domains. Difference Fourier maps were calculated with CNS and used to locate electron density corresponding to bound peptides. The structures were built with O (*42*) and refined with simulated annealing and energy minimization in CNS (*41*). Peptide positions were verified with simulated annealing omit maps (Figure 1). Final refinement statistics are given in Table 1.

Isothermal Titration Calorimetry. Wild-type, N165A, and N165D Sir2Tm proteins were dialyzed against a buffer solution containing 50 mM Tris-HCl (pH 8.0), 50 mM NaCl, and 0.5 mM TCEP prior to analysis. All ITC measurements were carried out using a MicroCal VP-ITC isothermal titration calorimeter (MicroCal, Inc.). A 0.08 mM solution of Sir2Tm diluted in sample buffer was added to the sample well, and a 0.8−1.6 mM solution of peptide made up in sample buffer was loaded into the injection syringe. For each experiment, a 60 s delay at the start of the experiment was followed by 25 injections of 10 μL of the titrant solution, spaced 240 s apart. The sample cell was stirred at 300 rpm throughout and maintained at a temperature of 25 °C. Control titrations were performed by titrating titrant solutions into dialysis buffer. Titration data were analyzed by correcting for baseline heats of dilution using Origin version 5.0 supplied by MicroCal Inc. The corrected data were fit to a theoretical titration curve describing one binding site per titrant. The area under each peak of the resultant heat profile was integrated and plotted against the molar ratio of Sir2Tm protein to titrant. A nonlinear best-fit binding isotherm for the data was used to calculate the protein:titrant stoichiometry, dissociation constant, and standard change in enthalpy.

RESULTS

Crystallization and Structure Determination of Sir2Tm Complexes. We attempted to cocrystallize Sir2Tm with six different acetylated substrates and one unacetylated peptide product (Table 2). Three of the peptides were derived from known sirtuin substrates. Two of the peptides correspond to an 18-residue sequence derived from the C-terminal domain of the p53 tumor suppressor, which is a substrate of the human sirtuin, SirT1. One peptide corresponds to the unacetylated state of Lys 382 (p53-K382), while the other corresponds to the acetylated state (p53-K382ac). The other peptide derived from known sirtuin substrates corresponds to the N-terminal tail of histone H4 acetylated at Lys 16 (H4-K16ac), which is a known in vitro and in vivo substrate for the yeast Sir2 protein (*1*). In addition, we set up crystallization trials with putative peptide substrates derived from loop regions of the histone core domain: histone H4 acetylated at Lys 77 (H4-K77ac) and Lys 79 (H4-K79ac), histone H3 acetylated at Lys 115 (H3-K115ac), and histone H2B acetylated at Lys 82 (H2B-K82ac). These peptides were chosen because of the recent finding that these sequences can be acetylated in vivo (*43*) and because they are located

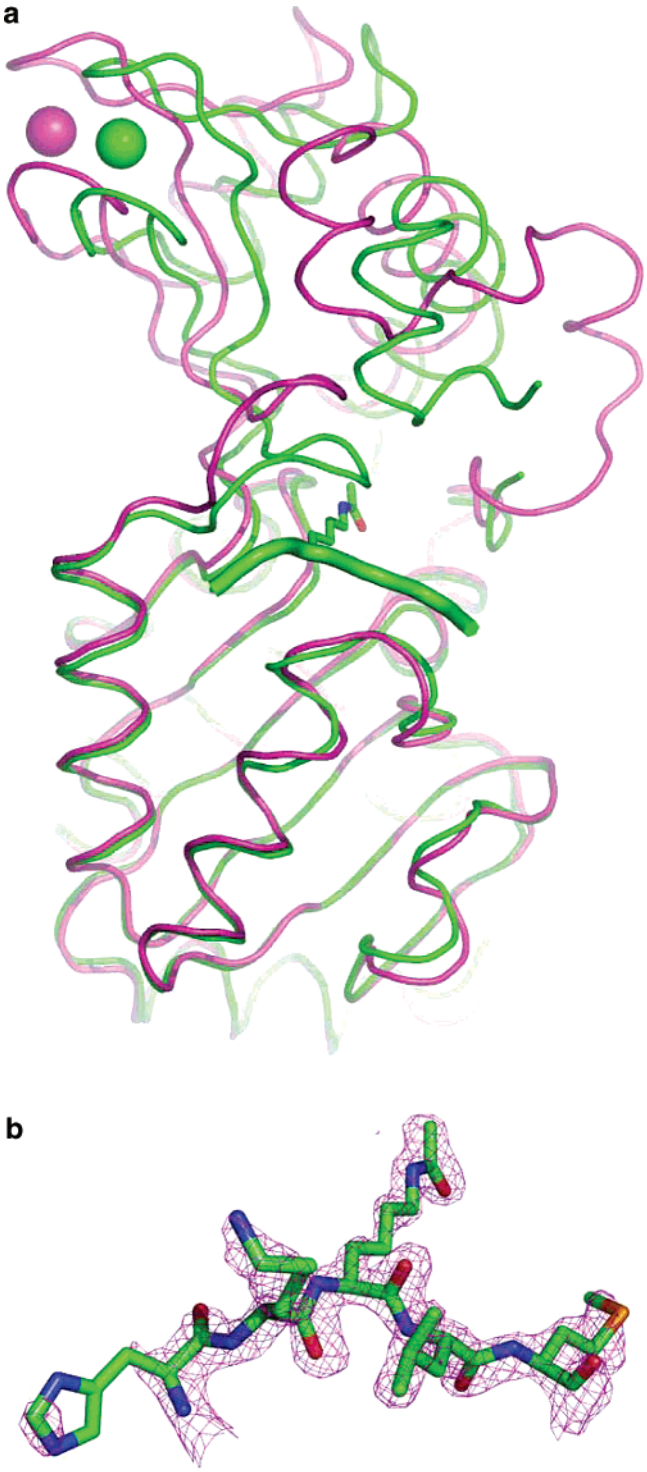

FIGURE 1: Crystal structures of Sir2Tm in the peptide-bound and unbound forms. (a) Superposition of backbone atoms of Sir2Tm−PPG crystals (magenta) and Sir2Tm bound to the p53-K382ac peptide (green). Superpositions were conducted by aligning the Cα atoms in the large domain. The position of the peptide is indicated by the thick green line. The acetyllysine is shown for reference. The green and magenta balls represent the positions of Zn^{2+} bound to the zinc binding domain. (b) Representative $F_o - F_c$ simulated annealing omit map showing peptide density for the p53-K382ac complex at 3σ.

in histone L2 loop regions on the lateral surface of the nucleosome core particle where they are likely to regulate histone−DNA contacts (*44*). Interestingly, the histone loop peptides share some sequence similarities with the histone H4 tail that is a known substrate for yeast Sir2, H4-K16ac

Table 2: Summary of Peptide Sequences and Thermodynamic Binding Constants for Wild-Type, N165D, and N165A Sir2Tms

Substrate	Sequence (-1 +2)	Crystallized	$Sir2Tm^{Wild\text{-}type}$ K_d (μM)	$Sir2Tm^{N165D}$ K_d (μM)	$Sir2Tm^{N165A}$ K_d (μM)
P53-K382	KKGQSTSRHKK LMFKTEG	yes	> 1000	>1000	>1000
P53-K382ac	KKGQSTSRHK**K**^{ac}LMFKTEG	yes	4.3 ± 0.5	1.5 ± 0.23	3.8 ± 0.7
H3-K115ac	HA**K**^{ac}RVTIQKKD	yes	9.2 ± 1.6	15.2 ± 3.2	8.6 ± 0.5
H4-K79ac	HAKR**K**^{ac}TVTSLD	yes	10.5 ± 1.4	5.5 ± 0.8	17.0 ± 3.1
H4-K77ac	HA**K**^{ac}RKTVTSLD	no	13.1 ± 1.8	47.8 ± 18.8	58.7 ± 11.4
H2B-K82ac	YN**K**^{ac}KSTISARE	no	ND[a]	185.8 ± 49.1	76.2 ± 15.7
H4-K16ac	GA**K**^{ac}RHRKILRD	no	1.1 ± 0.3	3.7 ± 1.6	2.0 ± 0.5

[a] Not determined.

(Table 2). With the exception of the unacetylated p53 peptide, all of the peptides are in vitro substrates for the bacterial sirtuin, Sir2Tm, as well as yeast Sir2, yeast Hst2, and human SirT1 enzymes (data not shown).

Crystallization trials were set up for Sir2Tm in the presence of 5 mM peptide (see Materials and Methods). Of the seven peptide−Sir2Tm complexes assayed in a sparse matrix crystallization screen, four yielded crystals under multiple conditions (Table 2). The crystals diffracted X-rays to resolutions that ranged from 1.6 Å for the H3-K115ac complex to 2.3 Å for the complex with unacetylated p53 peptide (Table 1). The structure of each peptide complex was determined by molecular replacement as described in Materials and Methods. The resulting electron density maps allowed us to place the acetyllysine and at least two residues N- and C-terminal to the acetyllysine in each structure.

Crystallization trials with apo-Sir2Tm failed to produce crystals. However, trials conducted in the presence of the coenzyme NAD^+ produced crystals that diffracted to 1.9 Å (Table 1). When the structure was determined, it was discovered that the structure lacked density consistent with a bound NAD^+ molecule but instead contained a sulfate ion bound in the NAD^+ binding site and a polypropylene glycol (PPG) molecule that stretched from the hydrophobic tunnel to the NAD^+ binding site. Since this structure of Sir2Tm lacks evidence of NAD^+ binding and because the angle between large and small domains more closely resembles that of the apoenzyme form of the human SirT2 structure (*28*) and the apoenzyme form of the Sir2 from *A. fulgidus* (*25*), we believe that the Sir2Tm−PPG structure is a close approximation of the apoenzyme form of Sir2Tm.

Overall Structure of Sir2Tm in Apoenzyme and Peptide-Bound Forms. The overall structure of Sir2Tm is topologically and structurally similar to that of previously reported structures of bacterial (*32*), archaeal (*27*, *29*), yeast (*30*), and human orthologs (*28*). The structure consists of a large pyridine dinucleotide binding domain, known as a Rossman fold domain, connected to a small zinc binding domain by a flexible loop that is disordered in the peptide-bound forms. The cleft that is formed between domains makes up the peptide substrate binding site, which binds in an extended conformation, completing a β-sheet interaction between conserved residues from the small and large domains. This motif has been called a "β-staple", referring to the way in which peptide binding tethers the interaction between the large and small domains (*27*). Comparison of peptide-bound and apoenzyme forms of Sir2Tm suggests that peptide binding induces a significant shift in the position of the small domain relative to the large domain, bringing the two domains together to form the β-staple motif (Figure 1). This shift is apparent in superpositions of the apoenzyme with the peptide-bound form. Whereas individual large and small domains of the peptide-bound and apoenzyme forms superimpose well, with root-mean-square differences (rmsd) in Cα positions of 0.8 and 0.6 Å, respectively, superpositions using the entire two-domain enzyme as a single rigid body are poor, with a rmsd of 12.1 Å, due to the relative change in orientation between the two domains. This shift was previously predicted on the basis of a comparison of different sirtuin homologues in differently liganded states (*27*). Taken together, these observations imply that peptide binding induces closure of the cleft between large and small domains of sirtuins. This results in the correct positioning of conserved residues for formation of the acetyllysine binding tunnel, as described below.

Structures of Sir2Tm Bound to Acetylated and Unacetylated Peptides. All peptide-bound Sir2Tm structures crystallize isomorphously (see Table 1) and are essentially superimposable, with an average rmsd of ∼0.4 Å for Cα atoms. The overall features of the Sir2Tm−peptide complexes are similar to those described for previously described structures (*27*, *31*, *32*). The acetyllysine binds in a conserved hydrophobic tunnel, forming van der Waals interactions with surrounding side chains as well as a single hydrogen bond

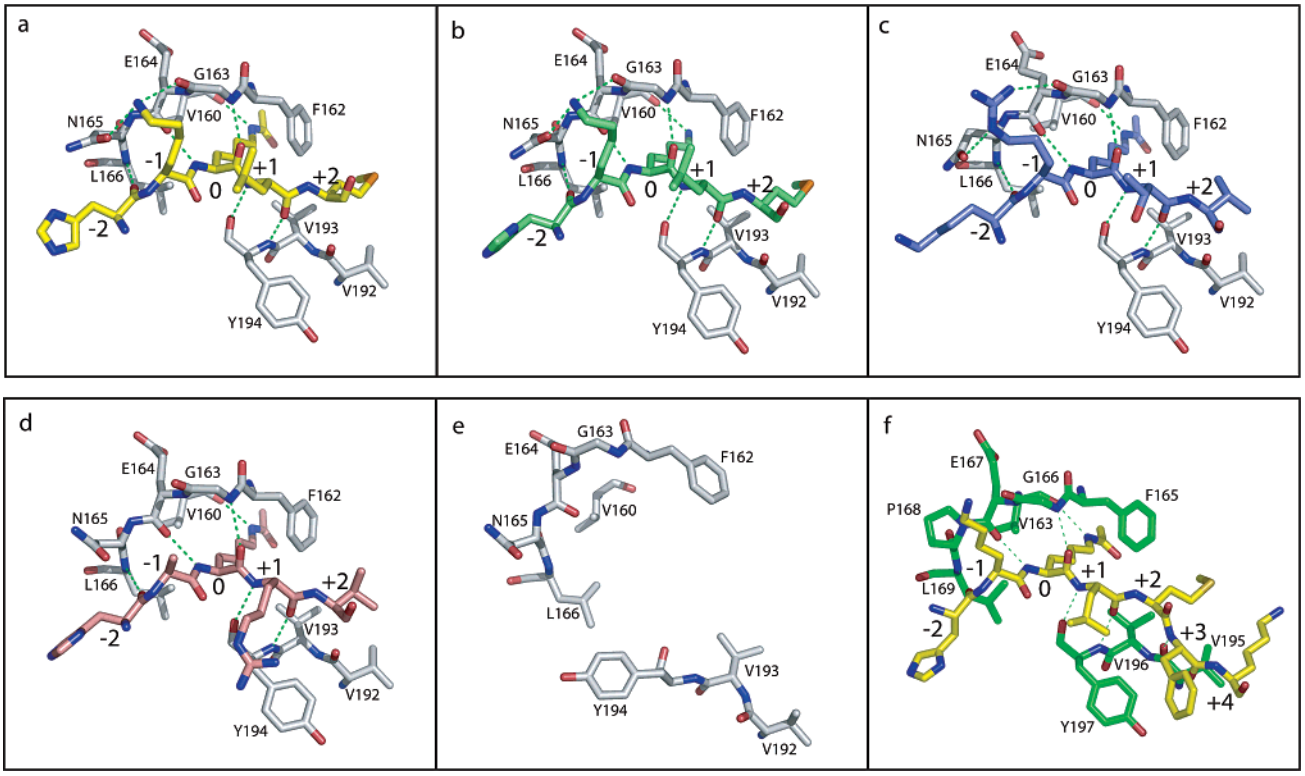

FIGURE 2: Peptide binding cleft of Sir2Tm showing specific interactions with the peptides used in this study. Panels show the active sites of Sir2Tm bound to (a) the p53-K382ac peptide, (b) the p53-K382 peptide (unacetylated), (c) the H4-K79ac peptide, (d) the H3-K115ac peptide, and (e) the apoenzyme. Panel f shows the p53-K382ac peptide bound to the archaeal sirtuin, Sir2 Af2 (*27*). This panel shows two additional p53 residues (+3 and +4) that are ordered in the Sir2 Af2 structure. Hydrogen bonds are shown as green dashed lines. Peptide residue positions are labeled with acetyllysine at position 0, N-terminal residues with negative numbers, and C-terminal residues with positive numbers. Sir2Tm residues that interact with the peptide are labeled with conventional single-letter amino acid designations.

between the Nϵ atom of the acetyllysine and the backbone carbonyl of Val 160. The peptides form a series of main chain hydrogen bond interactions with flanking strands in the large and small domain. Figure 2 summarizes the interactions in each peptide complex.

In addition to the β-sheet-like interactions noted above, side chains flanking the acetyllysine interact with residues in the enzyme in a peptide sequence-dependent manner. In particular, the residue immediately N-terminal to the acetyllysine, which we call peptide position −1, and the peptide residue two residues C-terminal to the acetyl lysine (peptide position +2) appear to govern sequence specific interaction. These interactions have not been observed in previously determined structures. Three of the four peptide-bound forms show hydrogen bond interactions between the amino acid in peptide position −1 and the side chain of Asn 165 and the main chain carbonyl of Gly 163 (Figure 2a−c). In the p53-K382ac peptide complex, for example, the ϵ-amino group of the lysine residue at position −1 of the peptide is 3.1 Å from the carbonyl oxygen of the carboxamide of Asn 165 and 2.9 Å from the main chain carbonyl of Gly 163 (Figure 2a). Similar interactions are observed in Sir2Tm complexes with the p53-K382 and H4-K79ac peptides. All four peptide complexes show additional hydrophobic and van der Waals interactions between the residue at position +2 of the peptide and the side chains of conserved sirtuin residues Phe 162 and Val 193 (Figure 3). For example, Cβ of the methionine in position +2 of the p53-K382ac and p53-K382 complexes is in van der Waals contact with Cϵ1 of Phe 162. Similarly, Cγ of the +2 methionine contacts Cγ2 of Val 193 in the p53-K382ac and p53-K382 complexes (Figure 3a). In the two structures with peptides containing a valine at position +2 (H3-K79ac and K3-K115ac), the valine Cγ2 methyl is located 3.3 and 3.9 Å from Cϵ1 of Phe 162, respectively, and 4.5 and 3.9 Å form Cγ1 of Val 193, respectively (Figure 3b).

The bridging van der Waals interactions between the peptide side chain at position +2 and enzyme residues Phe 162 and Val 193 that flank the substrate peptide may help stabilize β-staple formation and cleft closure that is observed when the peptide binds. For example, while the distance between Phe 162 and Val 193 is shortened by at least 2 Å when the peptide binds, the distance between these residues is still too great for van der Waals interactions (>4 Å). These hydrophobic and van der Waals interactions between the enzyme and residue position +2 help bridge interactions between opposite strands of the β-staple and likely contribute to the overall energy required for domain closure when a peptide binds.

We also observed several unique features among the peptide complexes. The complex of Sir2Tm with the p53-K382ac peptide shows continuous density for the main chain atoms of several additional residues N-terminal to the peptide binding site (residues 373−379). This stretch of residues forms an α-helix that projects away from the enzyme and is stabilized in the crystal by contacts with two symmetry-related molecules. The side chain for the arginine at position −3 is well-ordered and forms direct and water-mediated interactions with the side chain of Glu 198. The −3 arginine side chain is also stabilized by hydrogen bond interactions with Tyr 155 from a symmetry-related molecule. The structure of the complex with the deacetylated version of

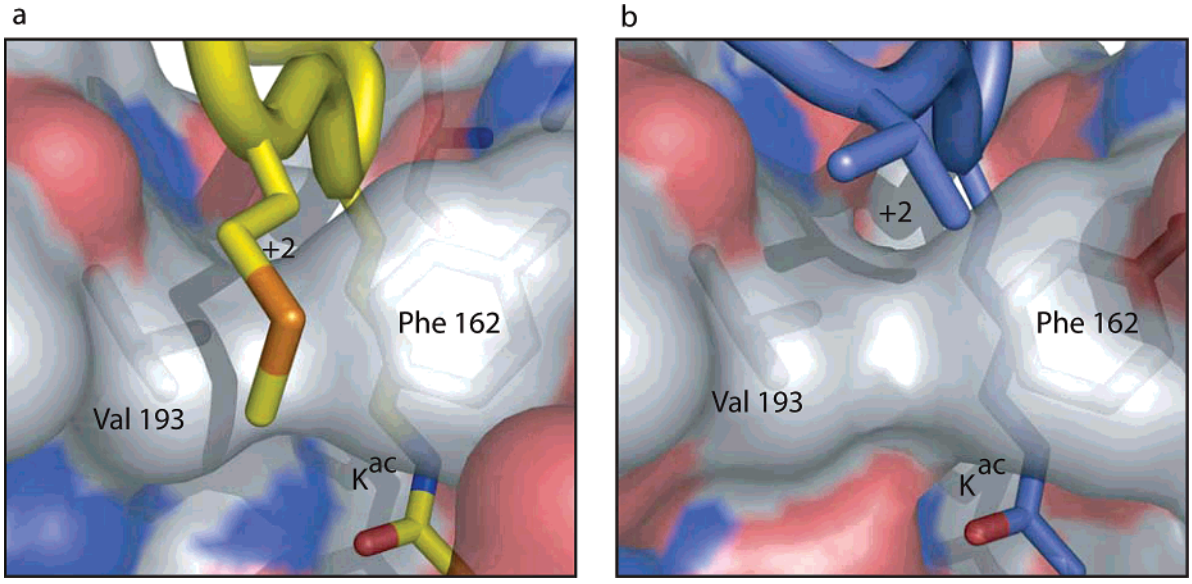

FIGURE 3: Transparent surface representations of interactions of peptide position +2 with Sir2Tm. (a) The p53-K382ac−Sir2Tm complex showing interactions of the +2 methionine with conserved residues Val 193 and Phe 162 in Sir2Tm. (b) The H4-K79ac−Sir2Tm complex showing interactions with the peptide +2 valine and the same conserved residues in Sir2Tm.

the same peptide (p53-K382) did not show the same interactions, and the N-terminal residues were consequently not ordered. One other unique feature observed in the structure of the H3-K115ac peptide complex is that the electron density map showed features consistent with an additional metal ion with tetrahedral coordination geometry, consistent with that of a zinc ion. This metal ion is coordinated by the imidazole moiety of the N-terminal histidine residue of the bound peptide, and by His 56 and Glu 58 from a symmetry-related molecule. A water molecule fills the last coordination sphere. While the metal binding in the crystal is clearly facilitated by crystal packing, it is possible that similar interactions could occur when Sir2Tm binds a peptide within a larger substrate.

Comparison of Substrate- and Product-Bound Forms of Sir2Tm. Analysis of the structures of Sir2Tm bound to both the acetylated and deacetylated p53-K382 peptide allows us to compare the way in which the enzyme binds to both peptides. Overall, the two structures are highly similar and superimpose with an rmsd for Cα atoms of 0.43 Å. The greatest difference occurs in the acetyllysine binding tunnel, where the acetyl group on Lys 382 in the p53-K382ac complex is replaced with a bound water molecule that is 3.25 Å from Nϵ of the unacetylated Lys 382. Interestingly, despite the presence of five lysine residues in the unacetylated p53-K382 peptide product, the peptide binds to Sir2Tm in an orientation identical to that seen in the structure containing the acetyllysine. As a result, the same interactions with flanking residues are present in both complexes (compare panels a and b of Figure 2).

It is notable that Sir2Tm selects K382 over the four other lysines in the unacetylated p53-K382 peptide for insertion into the hydrophobic tunnel. One possibility is that constraints imposed by crystal contacts determine the register in which the peptide binds to Sir2Tm. Alternatively, Sir2Tm may select which residue from the peptide to insert into the hydrophobic tunnel on the basis of specific side chain interactions with the surrounding peptide sequence. Since the N- and C-termini of the peptides bound to sirtuins are

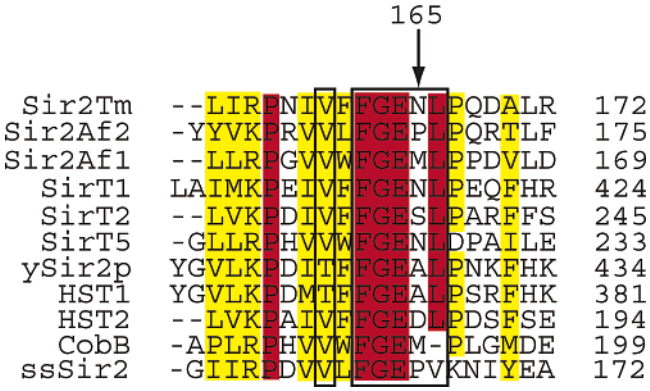

FIGURE 4: Sequence alignments of several sirtuins in the peptide binding region around Asn 165. The position of residue 165 (Sir2Tm numbering) is indicated with the arrow. Conserved and semiconserved residues are highlighted in red and yellow, respectively. Sir2Tm residues interacting with the peptide are boxed.

disordered in most structures described here and elsewhere and do not participate in crystal contacts, it appears likely that the selectivity for binding of a particular lysine within the hydrophobic tunnel is governed by sequence specific interactions between the enzyme and residues flanking the acetyllysine.

Thermodynamic Binding Analysis. The peptides that crystallized with Sir2Tm share several features that differ from peptides that failed to yield crystals. Peptides with a hydrophobic side chain at position +2 formed crystals, whereas those with a polar side chain at position +2 did not yield cocrystals with the enzyme. In addition, three of the four peptides that cocrystallized with Sir2Tm contain a lysine or arginine residue in the −1 position, which is a residue that forms complementary hydrogen bond interactions with the side chain of Asn 165. Since the identity of the residue at position 165 varies in different sirtuins (Figure 4), we reasoned that this interaction may be a mechanism for how different sirtuins discriminate among different substrates.

To test the role of Asn 165 in governing peptide affinity, we constructed two mutant forms of Sir2Tm that differ from

Table 3: Summary of Thermodynamic Binding Constants for Peptides that Vary at Positions −1 and +2

Substrate	Sequence (-1 +2)	Sir2Tm$^{Wild\text{-}type}$ K_d (μM)	Sir2Tm^{N165D} K_d (μM)
H4-K79ac	HAKR**K**^{ac}TVTSLD	10.5 ± 1.4	5.5 ± 0.8
H4-K79ac$^{R78A/V81K}$	HAKA**K**^{ac}TKTSLD	35.9 ± 2.6	134.4 ± 63.6
H4-K77ac	HA**K**^{ac}RKTVTSLD	13.1 ± 1.8	47.8 ± 18.8
H4-K77ac$^{A76R/K78V}$	HR**K**^{ac}RVTVTSLD	ND[a]	1.9 ± 0.06
H4-K77ac^{A76R}	HR**K**^{ac}RKTVTSLD	3.9 ± 0.5	2.3 ± 0.08
H4-K77ac^{K78V}	HA**K**^{ac}RVTVTSLD	15.9 ± 1.7	21.5 ± 2.6

[a] Not determined.

the wild-type enzyme at position 165 and then compared thermodynamic binding parameters using isothermal titration calorimetry (ITC) for the wild-type and mutant enzymes with the peptides used in this study. The results are summarized in Table 2. When Asn 165 is replaced with aspartate (Sir2Tm^{N165D}), the K_d for peptides with a lysine or arginine residue at peptide position −1 decreases 2−3-fold. By contrast, the K_d for peptides with an alanine at position −1 increases 2−4-fold. These results indicate that a negatively charged residue at position 165 increases the Sir2Tm affinity for peptides that contain a positively charged side chain at peptide position −1, but not for peptides with an alanine at position −1. When Asn 165 of Sir2Tm is replaced with alanine (Sir2Tm^{N165A}), dissociation constants remain the same or are increased up to 5-fold for the peptide complexes that were studied (Table 2). These results indicate that a Sir2Tm with an alanine at position 165 is not able to discriminate among this group of substrates. Therefore, the identity of the residue at position 165 in Sir2Tm likely plays an important role in sirtuin substrate recognition.

To further probe the role of specific side chain interactions in sirtuin affinity, we constructed peptides with substitutions at positions −1 and +2 and characterized their thermodynamic binding parameters with wild-type and Sir2Tm^{N165D} enzymes.We chose to introduce substitutions into the H4-K77ac and H4-K79ac peptides because they are identical in sequence but are acetylated at different lysines and because they exhibit distinct behavior in the sparse matrix crystallization screen used to assay crystallization conditions. While the H4-K79ac peptide produced multiple hits in sparse matrix screens for cocrystallization with Sir2Tm, the H4-K77ac peptide failed to yield crystals. These results suggest that the interactions of the H4-K79ac complex with positions −1 and +2 energetically favor Sir2Tm cocrystallization under the assayed conditions over the H4-K77ac complex, which have different residues at those positions.

To assay the sequence selectivity of wild-type and Sir2Tm^{N165D} enzymes, we constructed peptides with substitutions that swapped amino acids at positions −1 and +2 between the H4-K77ac and H4-K79ac peptides and assayed for changes in binding affinity by ITC. The results are summarized in Table 3. For the H4 peptide that crystallized with Sir2Tm (H4-K79ac), replacement of residues −1 and +2 with those found in H4 K77ac (H4-K79ac$^{R78A/V81K}$) results in 3- and 24-fold increases in the K_d values for peptide binding in the wild-type and N165D enzymes, respectively. These marked decreases in affinity are consistent with a central role for positions −1 and +2 of the peptide substrate in determining sirtuin substrate affinity. To verify that this was indeed the case, we made the reciprocal substitutions in the H4-K77ac peptide, changing the residues at positions −1 and +2 to those found in the H4-K79ac peptide (H4-K77ac$^{A76R/K78V}$), and measured this peptide's binding affinity in the N165D enzyme. As predicted, replacement of residues −1 and +2 in the wild-type H4 peptide sequence with Arg and Val increases the affinity of peptide binding by 25-fold.

To quantitate the individual roles of peptide positions −1 and +2 in enhancing the affinity of the H4-K77ac$^{A76R/K78V}$ peptide, we constructed two peptides with the individual substitutions (A76R and K78V) and measured their thermodynamic binding parameters with both wild-type and Sir2Tm^{N165D} enzymes (Table 3). The results show that when the Ala at peptide position −1 is replaced with an arginine in the H4-K77ac peptide (H4-K77ac^{A76R}), K_d decreases 3- and 21-fold for the wild-type and N165D enzymes, respectively. In contrast, when the Lys at peptide position +2 is replaced with a valine in the H4-K77ac peptide (H4-K77ac^{K78V}), K_d is not significantly altered when measured with the wild-type enzyme and decreases only 2-fold when measured with Sir2Tm^{N165D}. These results demonstrate the important role of peptide position −1 in sirtuin substrate affinity.

DISCUSSION

The structures of the different peptide−Sir2Tm complexes presented here reveal previously unobserved complementary

side chain interactions that contribute to our understanding of sirtuin substrate specificity. Previously determined crystal structures of sirtuin peptide complexes (*27*, *31*, *32*) showed that the binding of acetylated peptide substrates is governed by the insertion of the acetyllysine side chain into a highly conserved hydrophobic tunnel and by the formation of an enzyme−substrate β-sheet. The lack of specific side interactions in the substrate residues adjacent to the acetyllysine has led to the suggestion that domains outside the catalytic core of sirtuins may be necessary for sirtuin specificity (*32*). However, the observation that some sirtuins can distinguish between substrates that may contain multiple lysine residues that are acetylated suggests that the sirtuin catalytic core is sufficient for substrate recognition. For example, it has been shown that yeast Sir2p has preferential activity for a histone H4 peptide that is acetylated on Lys 16, as opposed to Lys 5, 8, and 12 (*1*). This is supported by (1) a recent steady-state kinetic analysis demonstrating that several different sirtuins display widely varying catalytic efficiencies with several different peptide substrates (*36*), (2) the recent demonstration that the human ortholog, SirT1, discriminates among substrates in a pentamer acetyl peptide library by as much as 20-fold (*37*), and (3) mutagenesis of surface side chain residues in the catalytic core of the archaeal homologue, Sir2Af1, that results in an increased affinity for a peptide derived from p53 (*27*). However, the rules that govern the substrate specificity of sirtuins have remained elusive, due in part to the lack of a systematic structural and thermodynamic analysis of different peptides within a single model system.

In this study, we compare the structural and thermodynamic properties of several different peptides using bacterial homologue Sir2Tm as a model system. This enzyme was chosen for this study because of its propensity to crystallize with various acetyllysine substrates and its robust in vitro catalytic activity. The peptides used in this investigation were derived from known physiological sirtuin substrates (the C-terminal tail of p53 and the flexible histone H4 N-terminal tail) as well as another class of peptides derived from the structured domain of several histones that in recent studies were shown to be targeted for acetylation (*43*, *44*). This latter class of peptides, derived from histone L2 loop regions, shares some sequence homology with the histone H4 N-terminal tail acetylated at Lys 16, a known substrate for Sir2p (*1*), suggesting that the structured domain of histones may also be sirtuin substrates. This is supported by recent studies showing that mutations in the histone H4 L2 loop residue, Lys 79, which was shown to be acetylated in mammals (*43*), partially phenocopy a Sir2 deletion in budding yeast (*45*, *46*). In addition, preliminary enzymatic assays with several different sirtuins and the histone L2 loop peptides used in this study show comparable activities with peptides derived from known sirtuin substrates (not shown), indicating that the histone L2 loop peptides are substrates for sirtuins in vitro. It remains to be determined if these L2 loop sequences are directly targeted by sirtuins in vivo.

It should be noted that while the length of the peptides used in this investigation varies between 11 and 18 residues, shortening the 18-residue p53-K382ac peptide to 12 residues does not significantly alter the K_d as measured by ITC (not shown). This suggests that peptide length differences do not account for the variability in binding affinity observed between the different lengths of peptides used in this investigation. In support of this, a recent investigation by Garske and Denu (*37*) shows that peptides varying in length between five and eight residues do not significantly differ in catalytic efficiency as measured by k_{cat}/K_m.

Comparison of the structures reported here reveals new side chain interactions that likely contribute to sirtuin substrate specificity. These interactions contribute to peptide binding through complementary hydrogen bond and van der Waals interactions with amino acids −1 and +2 of the peptide, respectively. While the thermodynamic binding analysis showed a relatively modest role for peptide position +2 in binding affinity, peptide position −1 exhibited a more striking effect. This residue forms hydrogen bond interactions with the nonconserved Asn 165 of Sir2Tm, which appears to be important for specificity. The importance of this interaction is demonstrated by the effect of mutation of the residue at position 165 in Sir2Tm. Mutagenesis of Asn 165 to aspartate results in an increased affinity for peptides with a lysine or arginine at position −1 (Table 2), presumably due to the addition of a salt bridge interaction. More dramatically, replacement of Ala at position −1 with arginine in the H4-K77ac peptide that did not crystallize increased the affinity of this peptide for N165D Sir2Tm by 21-fold and for wild-type Sir2Tm by ~3-fold. This confirms that the identity of the residue at position −1 of the peptide may be specifically recognized by sirtuins through complementary side chain interactions with the residue equivalent to position 165 in Sir2Tm.

Sequence alignments of sirtuins show that position 165 is a highly variable residue within an otherwise conserved stretch of amino acids that participate in peptide binding (Figure 4). The importance of this residue in peptide recognition is demonstrated by the structure of the p53-K382ac−Sir2Tm complex, in which Nϵ of the lysine side chain at peptide position −1 forms hydrogen bond interactions with the carbonyl oxygen of the side chain of nonconserved Asn 165 (Figure 2a). Although this peptide is not known to represent an in vivo substrate of Sir2Tm, we note that the human SirT1 enzyme, which targets the p53 tumor suppressor in vivo, also contains an Asn at position 165 (Sir2Tm numbering) (Figure 4). This suggests that this residue helps SirT1 to recognize peptide position −1 of the p53 C-terminal regulatory domain.

The importance of the residue in peptide position +2 is suggested by the crystal structures reported here and elsewhere. In this investigation, a common feature of the peptides that crystallized was the presence of a hydrophobic residue at peptide position +2. This residue forms van der Waals interactions with conserved residues Phe 162 and Val 193 from opposite strands of the β-staple motif. This suggests that sirtuins may in part select substrates on the basis of the identity of the residue at peptide position +2. This is supported by a recent investigation by Garske and Denu (*37*) that utilized a pentamer acetyl peptide library to identify sequences preferred by the human sirtuin ortholog, SirT1. They identified isoleucine and glutamine as amino acids that were preferred at peptide position +2. Isoleucine is expected to make contacts similar to those of valine and methionine, while glutamine may make contacts similar to those of methionine. However, in this investigation, replacement of the Lys at position +2 with valine in the H4-K77ac peptide

did not significantly alter the affinity of this peptide for wild-type TmSir2, although the K_d decreased 2-fold when the assay was conducted with N165D mutant Sir2Tm. It may be that peptide affinity is not significantly affected by a lysine to valine substitution at peptide position +2 because the aliphatic portion of the lysine side chain may also form similar van der Waals interactions.

The importance of peptide position +2 is also suggested by the ternary complex crystal structure of the yeast Hst2 enzyme bound to a histone H4 peptide acetylated at Lys 16 (*31*), albeit by a mechanism different from that observed with Sir2Tm. In the Hst2 structure, peptide binding is partially stabilized by a hydrogen bond and a salt bridge between the peptide +2 histidine and semiconserved Glu 64 from the flexible loop of Hst2 that is disordered in several sirtuin structures, including all of the peptide-bound structures in this study. The van der Waals interactions between peptide position +2 and conserved Phe 162 and Val 193 residues observed in the Sir2Tm−peptide complexes are absent in the Hst2 complex, suggesting a different mechanism for recognition of peptide position +2. This may explain why in this study the H4-K16ac peptide had the highest affinity with Sir2Tm but did not crystallize. It may be that the flexible loop in Sir2Tm is ordered by a similar hydrogen bond interaction between the peptide +2 histidine in the H4-K16ac peptide and Gln 45 (equivalent to Glu 64 in Hst2) from the flexible loop. An ordered flexible loop may prevent the necessary crystal contacts for crystallization of Sir2Tm under the conditions that were tested. In contrast, in the crystal structure of the bacterial CobB enzyme bound to the same histone H4 peptide (*32*), Cβ of the peptide +2 histidine forms a van der Waals contact with the Cϵ2 atom of conserved Phe 190 (equivalent to Phe 162 in Sir2Tm), suggesting that binding of the histone peptide to the bacterial enzyme is partially stabilized by a mechanism similar to that of Sir2Tm. Regardless of the mechanism, these results underscore the importance of peptide position +2 for side chain specific interactions that may help sirtuins distinguish among different substrates. A systematic kinetic, thermodynamic, and structural analysis of peptides with different residues at peptide position +2 will be required to improve our understanding of the quantitative role of peptide position +2 in sirtuin specificity.

These results raise the question of why these interactions were not observed in previously reported structures of sirtuins bound to acetyl peptide substrates. Peptide position −1 interactions were not observed because the interacting residues present in Sir2Tm are different in Sir2 Af2 and Hst2 structures. For example, in the Sir2 Af2 structure, despite the presence of a lysine at position −1 of the peptide, the residue equivalent to Asn 165 in Sir2Tm is proline, which is not expected to make the hydrogen bond interactions observed in Sir2Tm. Likewise, in the structure of Hst2, which has an aspartate at the position equivalent to Asn 165 in Sir2Tm, the structure was determined with the peptide sequence derived from histone H4, which contains an alanine at position −1, again not expected to make the hydrogen bond interactions.

Our observations suggests a general framework for identifying sirtuin substrates and for distinguishing among several possible acetyllysine targets in proteins that contain multiple acetylated lysines. The potential interactions between position −1 of the peptide and the amino acid corresponding to residue 165 of Sir2Tm place constraints upon the lysine residues that a given sirtuin can deacetylate. Depending upon the identity of the amino acid at position 165 of the enzyme, certain substrates are likely to produce favorable interactions with the enzymes, whereas other substrates will not be deacetylated efficiently due to steric clashes or unfavorable electrostatic interactions. Indeed, an examination of sirtuins with known substrates indicates a complementary pairing between the enzyme residue at position 165 and the amino acid in substrate peptide position −1 (Table 4). In all cases, the enzyme−substrate complex is predicted to allow interactions between the enzyme residue at position 165 and the residue in peptide position −1. This may explain why a peptide derived from tubulin is such a poor substrate for the yeast Hst2 enzyme, whose in vivo substrate is not known, as compared to other, histone-derived substrates (*19*, *36*). Tubulin contains an aspartic acid at peptide position −1, which is likely repelled by the negatively charged aspartate located at position 187 in Hst2 (equivalent to position 165 in Sir2Tm). Hst2 is approximately 6000-fold less efficient in deacetylating a tubulin peptide, as judged by k_{cat}/K_m, as compared with the activity of Hst2 with a variety of histone peptide substrates (*36*). This is consistent with an important role for position −1 in determining sirtuin substrate specificity.

Table 4: Summary of Expected Interactions between Position −1 of Known Sirtuin Substrates and the Sirtuin Residue at the Position Equivalent to Position 165 in Sir2Tm

enzyme	substrate	peptide position −1	enzyme position 165	ref
ySir2	H4-K16ac	A	A	*1*
SirT1	p53	K	N	*12*, *13*, *47*
SirT2	tubulin	D	S	*19*
CobB	ACS	G	M	*18*
ssSir2	Alba	G	P	*48*
Hst2	??	??	D	

In conclusion, the experiments reported here begin to shed light on the molecular basis of sirtuin substrate affinity. It is likely that as structures of sirtuins bound to their native substrates are determined other features that contribute to sirtuin specificity will emerge. The interactions of peptide positions −1 and +2 reported here form the basis for understanding how the sirtuin catalytic core recognizes and deacetylates specific substrates.

ACKNOWLEDGMENT

We thank Clara Keilkopf, Allen Sickmier, Sandra Gabelli, and Lin woo Kang for technical advice. We thank James Iben for helping in the refinement of crystallization conditions for the Sir2Tm−PPG complex. We also thank Jef Boeke, Kevin Hoff, and Michael Eddins for helpful discussions, Hidekazu Takahashi for purified sirtuin enzymes, and Mario Amzel and Anthony Armstrong for ITC access and assistance. We thank M. Becker from beamline X25 at the Brookhaven National Synchrotron Light Source and K. Brewster from the Biocars beamlines at the Advanced Photon Source.

REFERENCES

1. Imai, S., Armstrong, C. M., Kaeberlein, M., and Guarente, L. (2000) Transcriptional silencing and longevity protein Sir2 is an NAD-dependent histone deacetylase, *Nature 403*, 795−800.

2. Chang, J. H., Kim, H. C., Hwang, K. Y., Lee, J. W., Jackson, S. P., Bell, S. D., and Cho, Y. (2002) Structural basis for the NAD-dependent deacetylase mechanism of Sir2, *J. Biol. Chem. 277*, 34489−98.
3. Jackson, M. D., and Denu, J. M. (2002) Structural identification of 2′- and 3′-O-acetyl-ADP-ribose as novel metabolites derived from the Sir2 family of β-NAD^+-dependent histone/protein deacetylases, *J. Biol. Chem. 277*, 18535−44.
4. Sauve, A. A., Celic, I., Avalos, J., Deng, H., Boeke, J. D., and Schramm, V. L. (2001) Chemistry of gene silencing: The mechanism of NAD^+-dependent deacetylation reactions, *Biochemistry 40*, 15456−63.
5. Tanner, K. G., Landry, J., Sternglanz, R., and Denu, J. M. (2000) Silent information regulator 2 family of NAD- dependent histone/protein deacetylases generates a unique product, 1-O-acetyl-ADP-ribose, *Proc. Natl. Acad. Sci. U.S.A. 97*, 14178−82.
6. Tanny, J. C., and Moazed, D. (2001) Coupling of histone deacetylation to NAD breakdown by the yeast silencing protein Sir2: Evidence for acetyl transfer from substrate to an NAD breakdown product, *Proc. Natl. Acad. Sci. U.S.A. 98*, 415−20.
7. Brachmann, C. B., Sherman, J. M., Devine, S. E., Cameron, E. E., Pillus, L., and Boeke, J. D. (1995) The SIR2 gene family, conserved from bacteria to humans, functions in silencing, cell cycle progression, and chromosome stability, *Genes Dev. 9*, 2888−902.
8. McMurray, M. A., and Gottschling, D. E. (2003) An age-induced switch to a hyper-recombinational state, *Science 301*, 1908−11.
9. Gottlieb, S., and Esposito, R. E. (1989) A new role for a yeast transcriptional silencer gene, SIR2, in regulation of recombination in ribosomal DNA, *Cell 56*, 771−6.
10. Bennett, C. B., Snipe, J. R., Westmoreland, J. W., and Resnick, M. A. (2001) SIR functions are required for the toleration of an unrepaired double-strand break in a dispensable yeast chromosome, *Mol. Cell. Biol. 21*, 5359−73.
11. Brunet, A., Sweeney, L. B., Sturgill, J. F., Chua, K. F., Greer, P. L., Lin, Y., Tran, H., Ross, S. E., Mostoslavsky, R., Cohen, H. Y., Hu, L. S., Cheng, H. L., Jedrychowski, M. P., Gygi, S. P., Sinclair, D. A., Alt, F. W., and Greenberg, M. E. (2004) Stress-dependent regulation of FOXO transcription factors by the SIRT1 deacetylase, *Science 303*, 2011−5.
12. Luo, J., Nikolaev, A. Y., Imai, S., Chen, D., Su, F., Shiloh, A., Guarente, L., and Gu, W. (2001) Negative control of p53 by Sir2α promotes cell survival under stress, *Cell 107*, 137−48.
13. Vaziri, H., Dessain, S. K., Ng Eaton, E., Imai, S. I., Frye, R. A., Pandita, T. K., Guarente, L., and Weinberg, R. A. (2001) hSIR2-(SIRT1) functions as an NAD-dependent p53 deacetylase, *Cell 107*, 149−59.
14. Araki, T., Sasaki, Y., and Milbrandt, J. (2004) Increased nuclear NAD biosynthesis and SIRT1 activation prevent axonal degeneration, *Science 305*, 1010−3.
15. Picard, F., Kurtev, M., Chung, N., Topark-Ngarm, A., Senawong, T., Machado De Oliveira, R., Leid, M., McBurney, M. W., and Guarente, L. (2004) Sirt1 promotes fat mobilization in white adipocytes by repressing PPAR-γ, *Nature 429*, 771−6.
16. Lin, S. J., Defossez, P. A., and Guarente, L. (2000) Requirement of NAD and SIR2 for life-span extension by calorie restriction in *Saccharomyces cerevisiae*, *Science 289*, 2126−8.
17. Kaeberlein, M., McVey, M., and Guarente, L. (1999) The SIR2/3/4 complex and SIR2 alone promote longevity in *Saccharomyces cerevisiae* by two different mechanisms, *Genes Dev. 13*, 2570−80.
18. Starai, V. J., Celic, I., Cole, R. N., Boeke, J. D., and Escalante-Semerena, J. C. (2002) Sir2-dependent activation of acetyl-CoA synthetase by deacetylation of active lysine, *Science 298*, 2390−2.
19. North, B. J., Marshall, B. L., Borra, M. T., Denu, J. M., and Verdin, E. (2003) The human Sir2 ortholog, SIRT2, is an NAD^+-dependent tubulin deacetylase, *Mol. Cell 11*, 437−44.
20. Fulco, M., Schiltz, R. L., Iezzi, S., King, M. T., Zhao, P., Kashiwaya, Y., Hoffman, E., Veech, R. L., and Sartorelli, V. (2003) Sir2 regulates skeletal muscle differentiation as a potential sensor of the redox state, *Mol. Cell 12*, 51−62.
21. Motta, M. C., Divecha, N., Lemieux, M., Kamel, C., Chen, D., Gu, W., Bultsma, Y., McBurney, M., and Guarente, L. (2004) Mammalian SIRT1 represses forkhead transcription factors, *Cell 116*, 551−63.
22. Cohen, H. Y., Miller, C., Bitterman, K. J., Wall, N. R., Hekking, B., Kessler, B., Howitz, K. T., Gorospe, M., de Cabo, R., and Sinclair, D. A. (2004) Calorie restriction promotes mammalian cell survival by inducing the SIRT1 deacetylase, *Science 305*, 390−2.
23. Yeung, F., Hoberg, J. E., Ramsey, C. S., Keller, M. D., Jones, D. R., Frye, R. A., and Mayo, M. W. (2004) Modulation of NF-κB-dependent transcription and cell survival by the SIRT1 deacetylase, *EMBO J. 23*, 2369−80.
24. Michishita, E., Park, J. Y., Burneskis, J. M., Barrett, J. C., and Horikawa, I. (2005) Evolutionarily Conserved and Nonconserved Cellular Localizations and Functions of Human SIRT Proteins, *Mol. Biol. Cell. 16*, 4623−35.
25. Avalos, J., Boeke, J. D., and Wolberger, C. (2004) Structural Basis for the Mechanism and Regulation of Sir2 Enzymes, *Mol. Cell 13*, 639−48.
26. Avalos, J. L., Bever, K. M., and Wolberger, C. (2005) Mechanism of sirtuin inhibition by nicotinamide: Altering the NAD^+ cosubstrate specificity of a Sir2 enzyme, *Mol. Cell 17*, 855−68.
27. Avalos, J. L., Celic, I., Muhammad, S., Cosgrove, M. S., Boeke, J. D., and Wolberger, C. (2002) Structure of a Sir2 enzyme bound to an acetylated p53 peptide, *Mol. Cell 10*, 523−35.
28. Finnin, M. S., Donigian, J. R., and Pavletich, N. P. (2001) Structure of the histone deacetylase SIRT2, *Nat. Struct. Biol. 8*, 621−5.
29. Min, J., Landry, J., Sternglanz, R., and Xu, R. M. (2001) Crystal structure of a SIR2 homolog-NAD complex, *Cell 105*, 269−79.
30. Zhao, K., Chai, X., Clements, A., and Marmorstein, R. (2003) Structure and autoregulation of the yeast Hst2 homolog of Sir2, *Nat. Struct. Biol. 10*, 864−71.
31. Zhao, K., Chai, X., and Marmorstein, R. (2003) Structure of the yeast Hst2 protein deacetylase in ternary complex with 2′-O-acetyl ADP ribose and histone peptide, *Structure 11*, 1403−11.
32. Zhao, K., Chai, X., and Marmorstein, R. (2004) Structure and substrate binding properties of cobB, a Sir2 homolog protein deacetylase from *Escherichia coli*, *J. Mol. Biol. 337*, 731−41.
33. Zhao, K., Harshaw, R., Chai, X., and Marmorstein, R. (2004) Structural basis for nicotinamide cleavage and ADP-ribose transfer by NAD^+-dependent Sir2 histone/protein deacetylases, *Proc. Natl. Acad. Sci. U.S.A. 101*, 8563−8.
34. Blander, G., and Guarente, L. (2004) The Sir2 family of protein deacetylases, *Annu. Rev. Biochem. 73*, 417−35.
35. Khan, A. N., and Lewis, P. N. (2005) Unstructured Conformations Are a Substrate Requirement for the Sir2 Family of NAD-dependent Protein Deacetylases, *J. Biol. Chem. 280*, 36073−8.
36. Borra, M. T., Langer, M. R., Slama, J. T., and Denu, J. M. (2004) Substrate specificity and kinetic mechanism of the Sir2 family of NAD^+-dependent histone/protein deacetylases, *Biochemistry 43*, 9877−87.
37. Garske, A. L., and Denu, J. M. (2006) SIRT1 top 40 hits: Use of one-bead, one-compound acetyl-peptide libraries and quantum dots to probe deacetylase specificity, *Biochemistry 45*, 94−101.
38. Smith, J. S., Avalos, J., Celic, I., Muhammad, S., Wolberger, C., and Boeke, J. D. (2002) SIR2 family of NAD^+-dependent protein deacetylases, *Methods Enzymol. 353*, 282−300.
39. Otwinowski, Z., and Minor, W. (1997) Processing of X-ray Diffraction Data Collected in Oscillation Mode, *Methods Enzymol. 276*, 307−26.
40. Vagin, A., and Teplyakov, A. (1997) MOLREP: An automated program for molecular replacement, *J. Appl. Crystallogr. 30*, 1022−5.
41. Brunger, A. T., Adams, P. D., Clore, G. M., DeLano, W. L., Gros, P., Grosse-Kunstleve, R. W., Jiang, J. S., Kuszewski, J., Nilges, M., Pannu, N. S., Read, R. J., Rice, L. M., Simonson, T., and Warren, G. L. (1998) Crystallography & NMR system: A new software suite for macromolecular structure determination, *Acta Crystallogr. D54* (Part 5), 905−21.
42. Jones, T. A., Zou, J. Y., Cowan, S. W., and Kjeldgaard, M. (1991) Improved methods for building protein models in electron density maps and the location of errors in these models, *Acta Crystallogr. A47* (Part 2), 110−9.
43. Zhang, L., Eugeni, E. E., Parthun, M. R., and Freitas, M. A. (2003) Identification of novel histone post-translational modifications by peptide mass fingerprinting, *Chromosoma 112*, 77−86.
44. Cosgrove, M. S., Boeke, J. D., and Wolberger, C. (2004) Regulated nucleosome mobility and the histone code, *Nat. Struct. Mol. Biol. 11*, 1037−43.
45. Hyland, E. M., Cosgrove, M. S., Molina, H., Wang, D., Pandey, A., Cottee, R. J., and Boeke, J. D. (2005) Insights into the role of histone H3 and histone H4 core modifiable residues in *Saccharomyces cerevisiae*, *Mol. Cell. Biol. 25*, 10060−70.

46. Park, J. H., Cosgrove, M. S., Youngman, E., Wolberger, C., and Boeke, J. D. (2002) A core nucleosome surface crucial for transcriptional silencing, *Nat. Genet. 32*, 273−9.
47. Langley, E., Pearson, M., Faretta, M., Bauer, U. M., Frye, R. A., Minucci, S., Pelicci, P. G., and Kouzarides, T. (2002) Human SIR2 deacetylates p53 and antagonizes PML/p53-induced cellular senescence, *EMBO J. 21*, 2383−96.
48. Bell, S. D., Botting, C. H., Wardleworth, B. N., Jackson, S. P., and White, M. F. (2002) The interaction of Alba, a conserved archaeal chromatin protein, with Sir2 and its regulation by acetylation, *Science 296*, 148−51.

BI0526332